Available online at www.sciencedirect.com
SCIENCE DIRECT®
International Journal of Heat and Mass Transfer 49 (2006) 4424–4436
International Journal of HEAT and MASS TRANSFER
www.elsevier.com/locate/ijhmt

Surface tension and frictional resistance of thermocapillary pumping in a closed microchannel

P.S. Glockner [a], G.F. Naterer [b,*]

[a] Department of Mechanical and Manufacturing Engineering, University of Manitoba, 15 Gillson Street, Winnipeg, Manitoba, Canada R3T 2N2
[b] Faculty of Engineering and Applied Science, University of Ontario Institute of Technology, 2000 Simcoe Street North, Oshawa, Ontario, Canada L1H 7K4

Received 3 June 2005; received in revised form 13 May 2006
Available online 3 July 2006

Abstract

This article investigates heat transfer and microfluidic forces on an enclosed droplet with thermocapillary pumping in a closed-ended microchannel. Numerical and theoretical formulations are developed to predict the droplet motion. Heat transfer through a silicon substrate to the droplet interface generates a thermocapillary force at the receding edge of the droplet. This thermocapillary force increases rapidly during a heating period, but decreases after the droplet moves past a thermal bridge. In the numerical formulation, a new pressure/velocity coupling is developed for the moving droplet/air interface. Close agreement between theoretical and predicted results of droplet displacement provides useful validation of the new formulations.

Keywords: Microchannel; Thermocapillary pumping; Surface tension; Friction

1. Introduction

In recent years, microelectromechanical systems (MEMS) have become the basis of a rapidly growing and profitable new industry. Some recent examples of innovative micro-devices are accelerometers for automobile airbags, keyless entry systems, dense arrays of optical mirrors for high-definition optical displays and scanning electron microscope tips to visualize single atoms [1]. Micro heat exchangers have been developed for convective cooling of microelectronic circuits [2,3]. MEMS have also been used in biomedical applications, such as microsystems for separating biological cells, blood analyzers and pressure transducers for catheters. Other recent advances have utilized EBSM (Entropy Based Surface Micro-profiling) for purposes of flow control, drag reduction and entropy generation minimization [4]. A comprehensive review of microfluidic transport phenomena was documented by Gad-el-Hak [1].

Microfluidic transport can be controlled by an applied pressure difference, electrical potential difference or thermocapillary pumping. Slip-flow conditions during microfluidic transport occur at sufficiently high Knudsen numbers [5]. Qu et al. [6] have investigated pressure-driven flow of water through trapezoidal microchannels. Various cross-sectional profiles of microchannels have been studied previously, including circular profiles of microtubes [7], rectangular microchannels exposed to a parallel freestream [4] and others. Unlike pressure driven systems, local changes of surface tension allow flow control by thermocapillary pumping (TCP) [8]. The thermal conductivity of the liquid affects the velocity of the micro-droplet during TCP motion [9]. An electrical analogy of thermocapillary pumping is electrocapillary transport, whereby an electrical potential gradient between two immiscible conducting fluids generates a spatial change of surface tension [10].

Recent studies by Sammarco and Burns [11] have reported that nano-sized droplets could be transported

* Corresponding author. Fax: +1 905 721 3370.
E-mail address: greg.naterer@uoit.ca (G.F. Naterer).

0017-9310/$ - see front matter © 2006 Elsevier Ltd. All rights reserved.
doi:10.1016/j.ijheatmasstransfer.2006.05.005

Nomenclature

A	interfacial area (m^2)
B	surface tension constant
c_p	specific heat (J/kg K)
F	force (N)
G	microchannel constant
h	convection coefficient (W/m^2 K)
H	microchannel height (m)
i	row number
j	column number
k	thermal conductivity (W/m K)
m	mass of droplet (kg)
P	pressure (Pa)
q''	heat flux (W/m^2)
R	gas constant (J/kg K)
t	time (s)
T	temperature (K)
u	x-velocity component (m/s)
v	y-velocity component (m/s)
V	volume (m^3)
x,y	Cartesian coordinates (m)

Greek symbols

α	thermal diffusivity (m^2/s)
μ	dynamic viscosity (kg/m s)
θ	contact angle (rads)
ρ	density (kg/m^3)
σ	surface tension (N/m)

Subscripts

a	air
b	bulk
c	capillary
f	friction
i	initial
L	left edge
o	surroundings
R	right edge
s	droplet/air interface

Superscripts

o	previous time step
m	previous iteration
$m+1$	new iteration

effectively by thermocapillary pumping through open microchannels. A single end of the nano-droplet was heated, thereby creating a difference of surface tension and fluid pressure across the two ends of the droplet. Droplet velocities up to 330 μm/s were measured for toluene ($\Delta T =$ 26 °C), while temperature differences between 10 and 70 °C were studied with mineral oil. Contact angle hysteresis was a limiting factor on the fluid velocities. Surface treatments or converging channels were suggested as possible ways of reducing or offsetting the limiting influences of hysteresis. Effects of such methods on local pressure losses can be effectively characterized by local tracking of the entropy production rates [12].

TCP has potential applications to biotechnology microdevices, such as flow control in microfluidic devices for lab-on-a-chip technology. Blood and urine samples are typically sent to labs for analysis of medical processes, which may take several days. Additionally, errors such as mislabelling and lost samples may hamper with processing of data. A lab-on-a-chip is a compact point-of-care clinical testing device, whereby all operations can be performed instantly on a small chip [13]. Nanoliter samples of fluid can be transported within the chip to various processing stages using TCP. Since the fluid does not contact any physical pumping mechanism, the sample would not be contaminated. Unlike conventional micro-pumps, an advantage of TCP is it can move fluid in either direction, depending on the location of the surface heat source.

Another innovative TCP application involves optical fibres, when a small moving micro-droplet can re-direct a light beam by refraction or reflection to a different path [14]. Once the beam enters the fiber, it can be trapped by these internal reflections. Thermocapillary transport can be used for an optical ''switch'' to re-direct light from one fiber to another fiber. The droplet in the microchannel would intersect the fiber-optic light beam. When the microdroplet moves to the position of the intersecting light beam, the beam is reflected to a different fiber. Recent numerical studies involving FLOW-3D simulations [14] have studied thermocapillarity in a 14-μm channel (heated at the bottom boundary) for optical fiber applications.

An analytical formulation of double-cell thermocapillary transport in a 2-D slot [15] has predicted the spatial development of two-cell structures. Uniformly spaced temperature contours agreed well with predictions based on heat conduction alone in the theoretical analysis. But CFD studies [14] have predicted surface amplitudes of thermocapillary convection to be notably less than values reported previously by Sasmal and Hochstein [16]. In addition to single-phase problems with thermocapillary pumping, surface tension forces have significance in various multiphase systems, such as nucleate pool boiling [17] and three-phase problems [18]. Unlike past studies involving surface tension gradients on suspended droplets in an open microchannel [11], this article presents new data involving cyclic theromcapillary droplet transport in a

closed-ended microchannel. Microfluidic forces on droplets transported by thermocapillary pumping will be investigated theoretically and numerically.

Unlike past studies with open microchannels, the thermocapillary pressure difference across a droplet is offset by internal resistance of fluid friction, as well as compressed and expanded air regions in the closed-ended microchannel. In this article, a micro-droplet is constrained between two gas chambers in the microchannel. Droplet displacement compresses the downstream gas, while expanding the upstream gas. This generates an adverse external pressure gradient across the droplet, which resists thermocapillary forces and provides a restoring force that eventually returns the droplet back to its equilibrium position. In practical applications, this external pressure may be used to set a warning signal, activate a thermal or optical "switch" (similar to a fuse) or regulate a flow control device, such as a valve.

2. Formulation of micro-droplet heating period

Consider heat transfer to a droplet in a closed channel with sealed ends (see Fig. 1) from an external source, through a thermal bridge embedded in a substrate. Thermocapillary pumping occurs when temperature dependent variations of surface tension, and differences between contact angles at both ends of the droplet, contribute to an effective pressure difference across the droplet. This difference induces fluid motion within the microchannel. When the droplet moves from left to right (see Fig. 1), the air pressure increases in the right section of the microchannel. During the cooling period when the heat source is turned off, this air pressure drives the droplet back towards its initial equilibrium position. A thin air gap between the thermal bridge and silicon substrate attempts to minimize lateral heat conduction, which would reduce the net heat input into the microchannel.

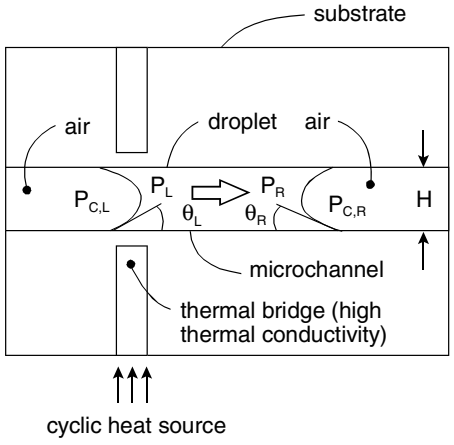

Fig. 1. Schematic (side view) of thermocapillary pumping of a liquid droplet between gas chambers in a closed-ended microchannel (not to scale).

Due to the complexity of this transient 2-D problem and the unknown conjugate boundary condition at the substrate/droplet interface, an analytical solution cannot be derived. Furthermore, the composite nature of the domain renders any general solution difficult. Each of the four phase regions (left air region, droplet, right air region and silicon substrate region) has different thermophysical properties. Additionally, heat transfer occurs within the liquid, solid and gas regions by coupled heat conduction and thermal convection. The thermal bridge transfers heat from the cyclic heat source to the droplet. Any theoretical predictions short of a full CFD solution would yield certain errors. Thus, the goal of the following theoretical model is predicting overall trends of the droplet motion, not the exact internal dynamics within a droplet. In this way, a simplified theoretical model can be used for global optimization studies. After certain global parameters are established, a detailed solution of the full Navier–Stokes equations can provide additional details regarding internal re-circulation within the moving micro-droplet.

In the following theoretical model, the droplet/air regions are approximated by two adjacent quasi one-dimensional semi-infinite domains. This approximation is supported by full numerical simulations, which indicate that convective cooling at the interface between the substrate and its surroundings is small compared to axial conduction across the domain. The heater is assumed to span the entire height of the microchannel in Fig. 1. In order to determine the magnitude of heat flow towards the left air/substrate region (left side of the heater) and droplet/substrate region (right side of the heater), it is assumed that each semi-infinite region has its own heat source at the interface. Then an interfacial condition is applied, whereby each region has the same interface temperature and the sum of heat flows from each region balances the total supplied heat flow from the thermal bridge. The thermal bridge cannot be accommodated in the theoretical model so it is not implemented in the numerical model when comparisons between the two solution methods are made. Additionally, the heat source is changed in the numerical model to match that of the theoretical model.

Under these assumptions, the heater becomes aligned with the left receding edge of the droplet. The interface temperature of either semi-infinite region, subject to a constant interfacial (surface) heat flux, q''_s, becomes

$$T(0,t) = T_i + \frac{2q''_s(\alpha t/\pi)^{1/2}}{k} \tag{1}$$

which may be written for the left and right sides of the heater as follows:

$$T_L(0,t) = T_i + \frac{2q''_{s,L}(\alpha_L t/\pi)^{1/2}}{k_L} \tag{2}$$

and

$$T_R(0,t) = T_i + \frac{2q''_{s,R}(\alpha_R t/\pi)^{1/2}}{k_R} \tag{3}$$

Equating temperatures in Eqs. (2) and (3) at the interface and re-arranging,

$$q''_{s,L}\frac{(\alpha_L)^{1/2}}{k_L}=q''_{s,R}\frac{(\alpha_R)^{1/2}}{k_R} \tag{4}$$

The total supplied heat flux from the thermal bridge matches the sum of heat flows from each region, so

$$q''_{s,R}=q''_s-q''_{s,L} \tag{5}$$

Using this heat balance in Eq. (4) yields the following result:

$$q''_{s,L}=\frac{q''_s(\alpha_R)^{1/2}/k_R}{(\alpha_L)^{1/2}/k_L+(\alpha_R)^{1/2}/k_R} \tag{6}$$

After the value of $q''_{s,L}$ is determined, then the value of $q''_{s,R}$ can be solved with Eq. (5). This procedure allows heat conduction within the domain to be modeled as two separate problems, with matching temperatures at the interface between both regions.

In the previous analysis, the values of α_L and α_R are properties of the composite material. The thermal conductivity of the left semi-infinite solid is approximated as

$$k_L=k_a\left(\frac{H_a}{H_t}\right)+k_s\left(\frac{H_s}{H_t}\right) \tag{7}$$

Also, the conductivity of the right semi-infinite solid is written as

$$k_R=k_d\left(\frac{H_d}{H_t}\right)+k_s\left(\frac{H_s}{H_t}\right) \tag{8}$$

where H is the combined height of the channel and the channel substrate. The subscripts 'a', 'd', 's' and 't' refer to air, droplet, substrate and total, respectively.

Then, the thermal diffusivity of the left semi-infinite domain can be estimated as

$$\alpha_L=\frac{k_L}{\rho_a c_{p,a}H_a/H_t+\rho_s c_{p,s}H_s/H_t} \tag{9}$$

Similarly, for the right semi-infinite region,

$$\alpha_R=\frac{k_R}{\rho_d c_{p,9}H_d/H_t+\rho_s c_{p,s}H_s/H_t} \tag{10}$$

In order to validate this assumption, thermocapillary pumping problems in Section 6 will be analyzed with both numerical (FVM; finite volume method) and theoretical methods. This section has considered the heating period when the droplet would be aligned above the thermal bridge. After it passes beyond the thermal bridge, a cooling period is encountered (next section).

3. Formulation of micro-droplet cooling period

The second stage of droplet motion occurs during the cooling period, after the receding edge of the droplet moves past the thermal bridge in Fig. 1. During the cooling period, a lumped capacitance approximation (called an LC Model) will be adopted, as a semi-infinite assumption is no longer adequate.

A non-uniform initial temperature distribution and unknown transient surface temperature/heat flux make a semi-infinite assumption unrealistic. The LC approximation neglects spatial temperature variations within the droplet, but predicts temporal changes of the receding edge temperature over time. This assumption is considered reasonable, in view of the tiny thermal mass of the micro-droplet. Though the dominant mode of heat transfer is axial conduction through the channel, the lumped capacitance considers convective cooling at the interface between the substrate and its surroundings. The portion of the domain considered in the LC Model is about 100 μm (length of the droplet) on either side of the heat source. Numerical simulations with the finite volume method confirmed that temperatures changed little outside of this range.

Based on the lumped capacitance assumption for cooling of the droplet [18]

$$T=T_o+(T_i-T_o)\exp\left[-\frac{hA_s t}{\rho V c_p}\right] \tag{11}$$

Alternatively,

$$t=\frac{\rho V c_p}{hA_s}\ln\left(\frac{T_i-T_o}{T-T_o}\right) \tag{12}$$

where T_i is the initial temperature in the cooling period. Also, A_s is the surface area exposed to the surroundings with a heat transfer coefficient of h at a temperature of T_o.

The value of h was approximated from the heating temperature profile of Eq. (1). The heating profile was considered in reverse, as a cooling curve from the point (T_c, t_c) to $(T_i, 0)$, where the subscript c refers to a critical point when the droplet has been displaced by a specified amount.

For example, (T_5, t_5) corresponds to conditions when the droplet is displaced by 5 μm. In this case, the approximation of the heat transfer coefficient during the cooling period becomes

$$h=\frac{\rho c_p V}{t_5 A_s}\ln(T_5-T_o) \tag{13}$$

where

$$\rho c_p=\frac{\rho c_{p,a}H_a+\rho c_{p,d}H_d+2\rho c_{p,s}H_s}{2H_t} \tag{14}$$

The previous analysis provides an approximation of the droplet temperature during the cooling period. Heating of the droplet is controlled by an external heater, while cooling of the droplet depends of the nature of the surroundings (substrate and adjacent air regions). Though the system state at the end of the heating period has major importance, a better approximation of the cooling period is needed. In Section 5, more detailed heat transfer simulations (during both heating and cooling periods) will be investigated numerically with the finite volume method.

4. Microfluidic forces of thermocapillary pumping

Fig. 1 illustrates a schematic of thermocapillary pumping (TCP) of a discrete droplet enclosed within a rectangular microchannel. Heat transfer to the left end of the droplet generates temperature variations within the liquid. The surface tension at an edge of the droplet varies with temperature, T, in the following manner:

$$\sigma = A - BT \tag{15}$$

where $A = 75.83$ dyn/cm and $B = 0.1477$ dyn/cm K for water. A large change of surface tension with temperature is desirable, as it would generate the largest pressure difference for a given heat input. This suggests that B in Eq. (15) is the most significant coefficient. But this article considers a closed-ended microchannel, so surface tension must overcome friction within the channel. As a result, a working fluid with a high B/μ ratio is also desirable. This article utilizes water as a working fluid, as water ($B/\mu = 15.5$ cm/s K) is more effective than other fluids (such as mineral oil, $B/\mu = 0.85$ cm/s K, or H_2O_2, $B/\mu = 12.4$ cm/s K) as a thermocapillary working fluid.

In the following theoretical model, consider an approximation whereby the droplet is treated as a non-deformable slug transported through a sealed channel. A heat source located at the receding edge of the droplet generates a thermocapillary force and fluid motion occurs from left to right in Fig. 1. During this droplet transport, the enclosed air section on the right side is compressed and the air on the left side is expanded. As a result, the rightward acceleration of the droplet in the sealed channel is lower, relative to a corresponding case for droplet motion in an open channel. Frictional resistance also reduces the rightward acceleration of the droplet. Based on the resulting net force (F), the droplet velocity (u) and displacement (x) can be determined from temporal integration over a discrete time step, Δt, of Newton's Second Law as follows:

$$u = u^o + \frac{F\Delta t}{m} \tag{16}$$

$$x = x^o + u\Delta t \tag{17}$$

where m and the superscript o refer to the droplet mass and previous time step, respectively. This approach will be called an SA Model (slug-flow approximation), as slug-like motion is predicted without internal distortion of the droplet. This simplified model will be compared afterwards to full numerical simulations of the Navier–Stokes equations within the droplet, in order to confirm the model's reliability.

The net force on the micro-droplet consists of a sum of three components, namely: (i) a thermocapillary force (F_c), (ii) external air force (F_a) and (iii) a frictional drag force (F_f).

4.1. Thermocapillary force (F_c)

The thermocapillary force is a transient force acting on the slug, which arises from a temperature difference and resulting surface tension difference across the slug. Axial heat conduction is assumed a dominant mode of heat transfer across the droplet, as it is several orders of magnitude larger than convective exchange with the surrounding substrate. The droplet length is much larger than its height, so heat conduction in a semi-infinite domain was approximated during the heating period (see Section 2).

Using temperatures calculated from Eq. (15), the variation of surface tension with temperature can be predicted. Then, the resulting thermocapillary force due the pressure difference across the droplet becomes

$$F_c = \Delta P_c A = (P_{c,R} - P_{c,L})A = GA\left[\left(\frac{\sigma\cos\theta}{H}\right)_R - \left(\frac{\sigma\cos\theta}{H}\right)_L\right] \tag{18}$$

In this equation, P_L and P_R are pressures on the left and right edges of the droplet, respectively. Also, θ is the contact angle between the liquid and solid wall (assumed to be zero) and H is the channel height. The value of G depends on the specific problem geometry. For example, $G = 4$ for a circular microtube, while $G = 2$ for slit-like microchannels and $G = 2(1 + \text{height/width})$ for square and rectangular microchannels.

4.2. External air force (F_a)

An external air force on the micro-droplet occurs from compression/expansion of the gas downstream/upstream of the droplet, respectively. For example, during droplet translation from left to right in Fig. 1, the compressed air exerts resistance on the droplet motion. The air was approximated as a perfect gas according to the ideal gas law ($PV = mRT$ where $R = 287$ J/kg K). The mass within each air region was calculated based on specified initial conditions, while the volume of each air region was determined from the droplet translation.

4.3. Frictional force (F_f)

The frictional force imposed on the slug by the channel walls was estimated from the steady-state velocity profile for Poiseuille flow, i.e.,

$$u = \frac{H^2}{2\mu}\frac{\partial P}{\partial x}\left[\left(\frac{y}{H}\right)^2 - \frac{y}{H}\right] \tag{19}$$

The bulk velocity, u_b, may be determined from Eq. (19). It becomes 2/3 of the centerline velocity, so

$$u_b = -\frac{H^2}{12\mu}\frac{\partial P}{\partial x} \tag{20}$$

A steady-state flow field is generated by a linear pressure gradient, so the pressure gradient, $\partial P/\partial x$, is assumed to have a constant value for a given time step. Then the frictional force on the slug can be approximated from Eqs. (19) to (20), after differentiating the velocity profile and

multiplying the resulting wall shear stress by the surface area of the wall/droplet interface, $2\Delta x b$, thereby yielding

$$F_f = \frac{12}{H}\mu \Delta x b u_b \tag{21}$$

This force resists thermocapillary motion of the micro-droplet from left to right in Fig. 1.

Combining the previous thermocapillary, air and friction forces gives the following net force on the micro-droplet,

$$F = GA\left[\left(\frac{\sigma\cos\theta}{H}\right)_R - \left(\frac{\sigma\cos\theta}{H}\right)_L\right] + AR\left[\left(\frac{m_a T_a}{V_a}\right)_L - \left(\frac{m_a T_a}{V_a}\right)_R\right] + A\Delta P \tag{22}$$

During the cooling period, the air force (second term on right side) assists the droplet motion, rather than resisting its motion. The previous theoretical results are called the SA Model (slug-flow approximation). In the next section, detailed CFD simulations of the full Navier–Stokes equations are developed for comparison purposes and validation of this theoretical formulation.

5. Numerical solution of thermocapillary pumping

In addition to the previous theoretical formulation, a finite volume method was developed to predict heat transfer within the accelerating droplet. The following 2-D transport equations of mass, momentum and energy are used to predict the fluid motion and heat transfer:

$$\frac{\partial}{\partial t}(\rho) + \frac{\partial}{\partial x}(\rho u) + \frac{\partial}{\partial y}(\rho v) = 0 \tag{23}$$

$$\frac{\partial}{\partial t}(\rho u) + \frac{\partial}{\partial x}(\rho u u) + \frac{\partial}{\partial y}(\rho v u) = -\frac{\partial p}{\partial x} + \frac{\partial}{\partial x}\left(\mu\frac{\partial u}{\partial x}\right) + \frac{\partial}{\partial y}\left(\mu\frac{\partial u}{\partial y}\right) + \dot{S}_u''' \tag{24}$$

$$\frac{\partial}{\partial t}(\rho v) + \frac{\partial}{\partial x}(\rho u v) + \frac{\partial}{\partial y}(\rho v v) = -\frac{\partial p}{\partial y} + \frac{\partial}{\partial x}\left(\mu\frac{\partial v}{\partial x}\right) + \frac{\partial}{\partial y}\left(\mu\frac{\partial v}{\partial y}\right) + \dot{S}_v''' \tag{25}$$

$$\frac{\partial}{\partial t}(\rho c_p T) + \frac{\partial}{\partial x}(\rho u c_p T) + \frac{\partial}{\partial y}(\rho v c_p T) = \frac{\partial}{\partial x}\left(k\frac{\partial T}{\partial x}\right) + \frac{\partial}{\partial y}\left(k\frac{\partial T}{\partial y}\right) + \dot{S}_T''' \tag{26}$$

A staggered grid SIMPLEC procedure was used to solve the coupled mass/momentum equations [19]. Droplet movement was accommodated by deforming grids in the air regions and a compliant sliding grid in the micro-droplet. Unlike past studies using a Poiseuille velocity profile within the droplet [11], the current simulations of the full Navier–Stokes equations allow more detailed information to be investigated (such as internal transient re-circulation within the micro-droplet).

Integrating Eq. (26) over a discrete control volume, V, and time step, Δt

$$\int_t^{t+\Delta t}\int_V \frac{\partial}{\partial t}(\rho c_p T)\,dV\,dt + \int_t^{t+\Delta t}\int_V \frac{\partial}{\partial x}(\rho u c_p T)\,dV\,dt + \int_t^{t+\Delta t}\int_V \frac{\partial}{\partial y}(\rho v c_p T)\,dV\,dt = \int_t^{t+\Delta t}\int_V \frac{\partial}{\partial x}\left(k\frac{\partial T}{\partial x}\right)dV\,dt + \int_t^{t+\Delta t}\int_V \frac{\partial}{\partial y}\left(k\frac{\partial T}{\partial y}\right)dV\,dt + \int_t^{t+\Delta t}\int_V \dot{S}_T'''\,dV\,dt \tag{27}$$

From left to right, the terms represent transient, convection (second and third terms), diffusion (fourth and fifth terms) and source terms, respectively.

The transient term is approximated with a backward difference in time, while Peclet weighted upwinding is adopted with upstream differencing in the convection terms [19]. Furthermore, linear interpolation and a lumped capacitance approximation are used for the diffusion and source terms, respectively. As a result, the discrete temperature equation becomes

$$a_P^T T_P = \sum a_{NP}^T T_{NP} + b_P^T \tag{28}$$

where

$$\sum a_{NP}^T T_{NP} = a_E^T T_E + a_W^T T_W + a_N^T T_N + a_S^T T_S \tag{29}$$

and

$$a_E^T = \max[0, (1-0.1|Pe_e|)^5]\frac{k_e A_e}{(\Delta x)_e} + \max(-\dot{m}_e, 0) \tag{30}$$

$$a_W^T = \max[0, (1-0.1|Pe_w|)^5]\frac{k_w A_w}{(\Delta x)_w} + \max(\dot{m}_w, 0) \tag{31}$$

$$a_N^T = \max[0, (1-0.1|Pe_n|)^5]\frac{k_n A_n}{(\Delta y)_n} + \max(-\dot{m}_n, 0) \tag{32}$$

$$a_S^T = \max[0, (1-0.1|Pe_s|)^5]\frac{\Gamma_s A_s}{(\Delta y)_s} + \max(\dot{m}_s, 0) \tag{33}$$

$$a_P^T = \frac{M_P}{\Delta t} + a_W^T + a_E^T + a_S^T + a_N^T \tag{34}$$

$$b_P^T = \frac{M_P^n}{\Delta t}T_P^n + \dot{m}_e - \dot{m}_w + \dot{m}_n - \dot{m}_s \tag{35}$$

In these equations, $\dot{m}$, Pe and M_P refer to the mass flow rate, Peclet number and mass within control volume P, respectively.

The numerical procedure for the solution of the fluid flow equations uses the SIMPLEC procedure [19], except that additional steps are needed for the adaptive moving grid in the micro-droplet and adaptive grid in the substrate. This solution procedure can be summarized by the following steps:

(1) calculate the new inlet and outlet boundary conditions for the droplet u-velocity,
(2) using the current pressure field, solve the momentum equations for the u and v fields,

(3) calculate the new pressure boundary conditions from current temperatures in the droplet,
(4) solve the pressure correction equation [19] to obtain the new pressure field,
(5) correct the u and v fields using the new pressure field,
(6) return to step (1) and repeat until the results converge within a specified tolerance.

In step (1), the value of the new u-velocity boundary condition matches the mass flow rate from the previous iteration. Unlike past numerical studies assuming a uniform pressure along the droplet/air interface [9], the current simulations specify only the corner pressures and predict the varying interfacial pressure resulting from the coupled pressure/velocity field in the SIMPLEC procedure [19].

At the interface between the substrate and the microchannel wall, a conjugate boundary condition is needed for coupled heat conduction in the substrate and convection in the fluid. This conjugate condition requires that the rate of heat conduction from the substrate matches the heat input into the moving droplet within the microchannel. After the droplet temperature is determined at the end of each time step, the droplet is translated and grids within the droplet and air regions are re-generated. As a result, the nodal points (where temperature values are saved) must be shifted. The mesh within the substrate must be updated to match the grid in the adjoining fluid region. In the substrate, the temperature field corresponding to the new mesh is linearly interpolated from values based on the previous mesh. In the vicinity of the thermal bridge, it is assumed that the heat flux between nodal points is constant, in order to approximate the temperature profile between nodal points. The substrate temperature, T_N, corresponding to the new x-location, x_N, is

$$T_N = T_L + \sum_{k=1}^{k=5} \frac{l_k}{L_k} \frac{R_k}{R_{TOT}} (T_R - T_L) \tag{36}$$

where T_L and T_R represent the left and right nodal temperatures (bounding T_N). Also, l/L is the fraction of each composite region "overtaken", R_k is the thermal resistance of a given region and R_{TOT} is the total thermal resistance between nodal points.

The mesh within the substrate is aligned with the mesh in the air and droplet regions. It is re-generated after each time step. As discussed previously, the temperature field within the substrate is linearly interpolated onto the new mesh, after the mesh is re-generated. Although a rectangular mesh with Cartesian coordinates is adopted in the air and droplet regions, the algorithm could potentially accommodate curvature of the droplet meniscus through a coordinate transformation at the droplet interface.

Heat transfer in the air adjacent to the droplet (see Fig. 1) involves both conduction and convection. The Navier–Stokes equations are solved within the moving micro-droplet, but the air velocities are approximated to vary linearly from zero at the walls to the droplet velocity at the droplet/air interface. Any air flowing out of a control volume within a time step is restored by the control volume, when the mesh is re-generated and the control volume is shifted. The velocity field within the droplet requires special consideration, in order to yield the correct advection terms within the discrete energy equation. This velocity field is solved in the reference plane of the overall system. This field resembles a developing channel flow. However, the mesh for the droplet is assumed to move within the domain at the droplet's bulk velocity. When viewed in the droplet's reference frame, a re-circulating velocity field is observed. This re-circulation involves a zero net mass flow in the x-direction. The droplet's velocity is considered in the reference frame of the droplet, when finding advecting velocities in the discrete equations. The droplet's bulk velocity is subtracted from the velocity field before calculating the advection terms.

In terms of boundary conditions, no-slip conditions were imposed along the substrate walls. Zero-flux conditions were specified at the left and right edges of the droplet for the v-velocity. Dirichlet boundary conditions were imposed along the left and right edges of the droplet for the u-velocity. The same value was specified at each node, in order to prevent distortion of the droplet. Values were selected to ensure that the mass flow rate along the left edge of the droplet matched the rate at the end of the previous iteration. In the following section, numerical simulations will be performed and compared against the theoretical formulation, in order to evaluate the reliability of the theoretical model.

6. Results and discussion

In this section, results from the theoretical and numerical formulations are presented for three cases, namely: (i) transient Poiseuille flow in a parallel channel, (ii) specified interface temperature and (iii) thermocapillary pumping in

Table 1
Problem parameters and thermophysical properties

Property	
Density of droplet	998 kg/m^3
Thermal conductivity of droplet	0.606 W/m K
Specific heat of droplet	4181 J/kg K
Kinematic viscosity of droplet	959×10^{-6} kg/m s
Density of air	1.16 kg/m^3
Thermal conductivity of air	0.0263 W/m K
Specific heat of air	1007 J/kg K
Density of substrate	2500 kg/m^3
Thermal conductivity of substrate	0.96 W/m K
Specific heat of substrate	837 J/kg K
Microchannel length	2 mm
Microchannel height	0.5, 1 and 2 μm
Microchannel depth	100 μm
Substrate height	20 μm
Droplet length	100 μm
Applied heat flux	5000 kW/m^2

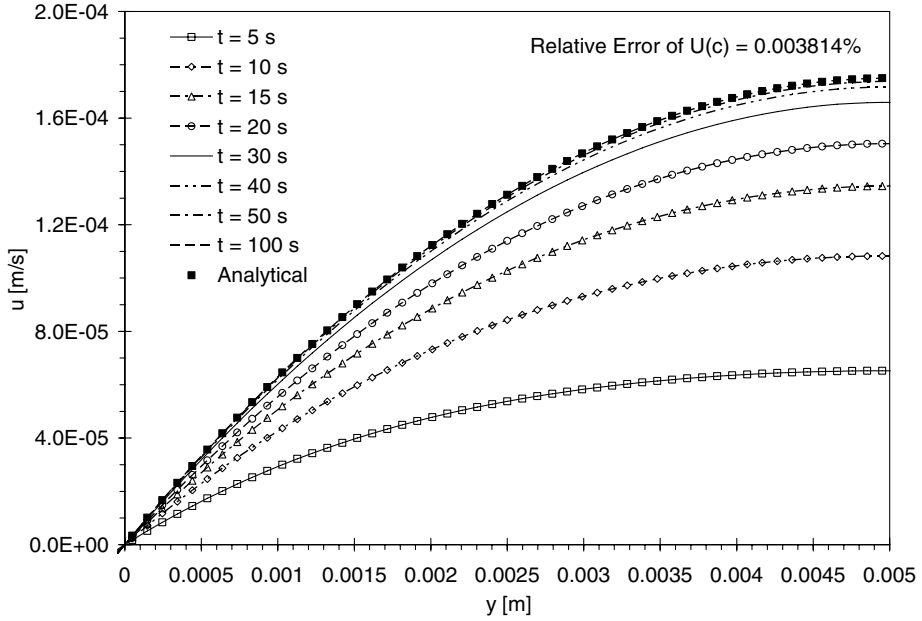

Fig. 2. Transient change of droplet velocity for Poiseuille flow in an open-ended microchannel.

a closed-ended microchannel. Problem parameters for cases (ii) and (iii) are summarized in Table 1.

6.1. Case 1: transient Poiseuille flow in a parallel channel

In the first case, consider a pressure difference that is suddenly applied to a motionless droplet in a parallel channel with a half-width of 5 mm. This transient Poiseuille-type flow becomes analogous to droplet acceleration when an externally applied heat input generates a sudden thermocapillary force on the droplet. As a result, this first test problem provides useful validation of the droplet flow formulation for impulsively driven motion using the FVM.

In Fig. 2, the fluid velocity changes over time, after the fluid accelerates from rest. The near-wall velocity gradient and wall shear stresses are increasing with time, so frictional resistance on the droplet is lowest when the droplet initially begins accelerating. After about 100 s, the droplet velocity approaches a steady state. It can be observed that close agreement between analytical (steady-state Poiseuille flow) and predicted results is obtained in Fig. 2, as the steady-state solution error is about 0.0038%.

6.2. Case 2: specified left and right edge temperatures (closed-ended microchannel)

For purposes of validation of the SA Model (slug-flow approximation), numerical simulations were compared against the SA Model for a simplified case of a constant temperature difference across the droplet. The air regions (upstream and downstream of the droplet) experience expansion and compression, respectively, when the droplet translates. Fig. 3a and b show a case in which the end temperatures are held constant at $T_L = 22\ ^\circ C$ and $T_R = 20\ ^\circ C$. In Fig. 3a, close agreement between theoretical and numerical predictions is achieved for the pressure difference

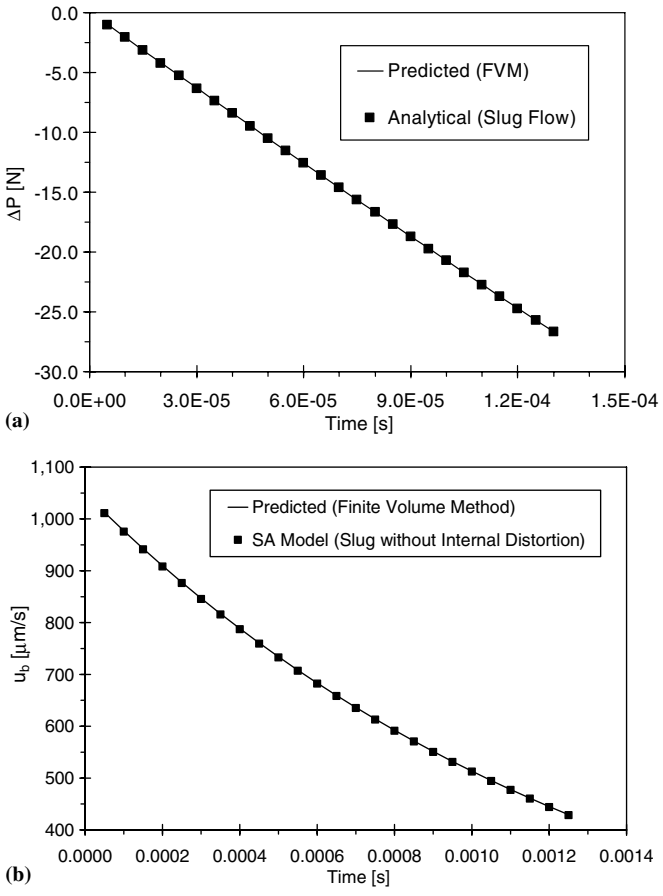

Fig. 3. (a) Pressure difference and (b) bulk velocity of discrete droplet in the closed-ended microchannel (note: velocity approaches zero as droplet nears its maximum displacement before heat source removed).

across the droplet. The specified temperature difference produces a constant thermocapillary force, which is offset by fluid friction along the walls and opposing gas pressures of the air in the left and right sections of the microchannel. These combined forces initially generate a nearly linearly decreasing pressure across the droplet (see Fig. 3a).

A higher liquid pressure at the receding edge of the droplet (due to reduced surface tension) yields a negative pressure difference in the streamwise direction of droplet motion. Although it cannot predict the detailed dynamics within a droplet, the slug-flow approximation in Fig. 3a provides good estimates of the overall pressure difference across the droplet. Given the correct temperature boundary condition for calculating the thermocapillary pressure, the theoretical model may be used to predict the droplet translation.

In Fig. 3a, the predicted velocity agrees closely with the SA Model during the heating period. The driving thermocapillary force is constant (due to the constant end temperatures). Fluid friction and compressed air oppose the rightward motion of the droplet. The net force is largest at time zero, when the friction and air forces are zero. The frictional force increases with velocity, while the air force increases with droplet displacement. The frictional force increases rapidly while the droplet accelerates and then decreases as the droplet's velocity is reduced by the opposing gas forces. The air force increases while the droplet translates from left to right in Fig. 1. Near the end of the heating period, when the droplet velocity (and thus friction) is small, the thermocapillary force nearly balances the opposing air force. When the droplet has been sufficiently displaced, the heat source is removed. Thermocapillary forces decrease rapidly and the gas pressure of the compressed air phase becomes sufficiently high to accelerate the droplet leftwards back towards its initial position.

Fig. 4 shows a case in which transient left and right droplet temperatures are specified in the theoretical model. The values of the temperatures are imported from a data file that was generated during corresponding FVM simulations. Numerical predictions are shown up to the time when the droplet has reached its peak displacement twice. These results include two complete heating/cooling cycles of the external heat source. Close agreement between the SA Model and FVM predictions of the micro-droplet displacement is observed in Fig. 4, thereby suggesting that the transient droplet end temperatures yield the proper driving force on the micro-droplet motion in the theoretical model. The peak displacement of the micro-droplet is about 5 μm, but this position could be readily controlled by varying the heat input, droplet size or gas volume within the microchannel.

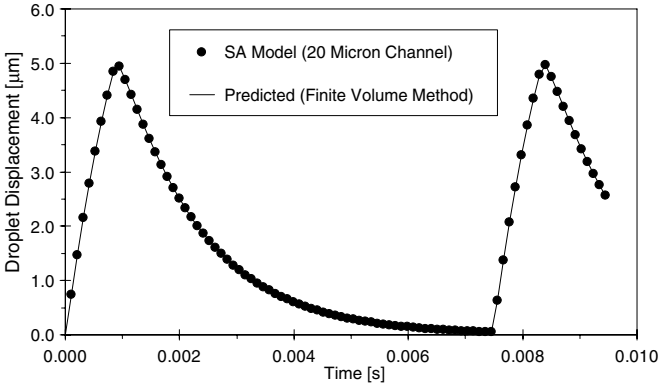

Fig. 4. Predicted droplet displacement in closed-ended microchannel (note: temperatures of droplet ends in the theoretical model are imported from a data file generated by the numerical simulation).

The cyclic heat source produces a rightward moving droplet during the heating period and a leftward droplet motion during the cooling period, when the cyclic heat source is turned off. It can be observed that the droplet returns almost completely to its initial position (zero reference position in Fig. 4). This ensures that the droplet transport could be sustained continually over time. It should be noted that cyclic heating/cooling is needed to allow the micro-droplet to return to its initial position. If the heater is not turned off, the opposing pressure of the compressed gas phase would be insufficient to drive back the droplet against an opposing thermocapillary force, with a continually heated region at the zero reference position.

In Fig. 4, moving 5 μm in 0.001 s translates to velocities of about 0.5 cm/s. The values have occurred as a result of the very small microchannel height. Sammarco and Burns [11] have derived the following expression for the steady-state droplet velocity corresponding to Poiseuille flow in open channels: $v = d^2\Delta P/S\mu L$. Using a pressure difference of $B\Delta T$ with B from Eq. (15), a temperature difference of approximately 40° (Fig. 4), and S equal to 12 for slit flow, this equation yields a steady state velocity of 2.048 cm/s. The adverse external pressure generated from the droplet motion (due to the closed ends of the microchannel) prevents the droplet from reaching its steady state velocity. Thus, the predicted velocity is not identical to the case studied by Sammarco and Burns [11], but it provides useful comparison with respect to the general order of magnitude of predicted velocities in Fig. 4.

6.3. Case 3: thermocapillary pumping in a closed-ended microchannel

After the fluid flow formulation was validated, a third problem of thermocapillary pumping in a closed-ended microchannel was investigated with the theoretical model. Effects of different channel heights on thermocapillary transport were considered. The thermocapillary force depends on the channel height, due to heat transfer within the fluids. Also, the external air force is proportional to the channel height. But it also depends on air temperature, volume and droplet displacement. From Section 4, the frictional force is inversely proportional to the channel height and it depends on the droplet velocity. The SA Model (Section 4) provides useful benefits, as it will be

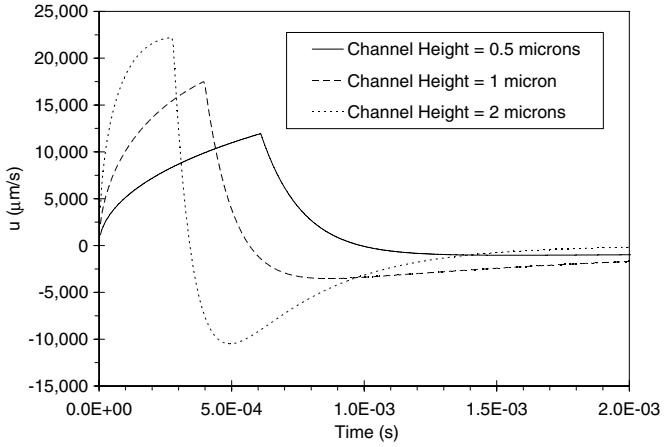

Fig. 5. Comparison of theoretical predictions of droplet velocity (heating and cooling periods) for three microchannel heights.

shown to provide reasonable estimates of these complex interactions without detailed CFD calculations.

Thermophysical properties and problem parameters in this test problem are summarized in Table 1. In the following results, various channel heights are examined. The heat source was turned off, after the droplet had moved a specified distance. Predicted results of the bulk droplet velocity are illustrated in Fig. 5. The peak velocity is highest with larger microchannels, since the net frictional resistance on the fluid motion becomes smaller. In each case, the droplet velocity is positive and increasing during early times, as the rightward thermocapillary force exceeds frictional resistance and the opposing gas pressures in the air sections of the closed-ended microchannel (see Fig. 1). The droplet begins decelerating when the opposing gas pressure and frictional forces become sufficiently large. The droplet reverses direction after it has been sufficiently displaced and the heat source is removed, at which time the thermocapillary force decreases rapidly. The velocity approaches zero towards the right side of Fig. 5, as the droplet returns back to its initial position. At that point, the heat input can be re-applied and the droplet motion can be re-initiated. These results suggest that a stationary heat source can be successfully used to generate cyclic transport of a droplet in a closed-ended microchannel.

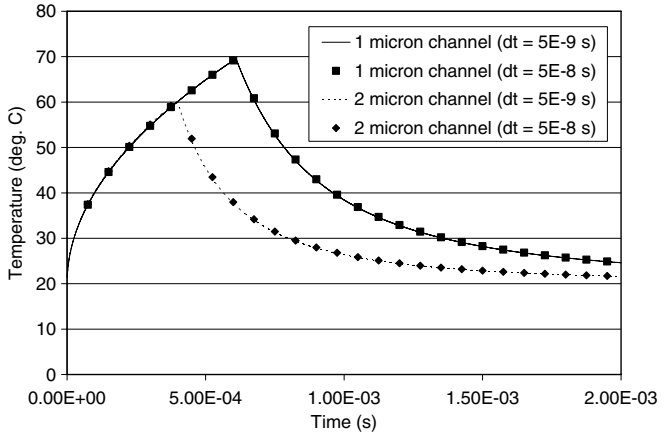

Fig. 6. Predicted temperature of the left droplet/air/substrate interface at varying time steps.

In Fig. 6, predicted temperatures at the left end of the micro-droplet are illustrated. Recall that in the actual FVM simulations of TCP, two-dimensional heat transfer would occur through the substrate from the thermal bridge (see Fig. 1). During this heating period, the temperature increases at the left end of the droplet and the droplet moves rightwards. Then it moves beyond the thermal bridge and the temperatures and thermocapillary forces decrease during the cooling period. Since there is no thermal bridge in the theoretical model, the heat source is simply removed after the droplet has been displaced by 5 μm. During this transition between heating and cooling periods, a certain time delay occurs before the thermal wave propagates to the right end of the droplet by heat conduction. As a result, the temperature increase at the right end of the droplet is delayed (relative to the left end) during the heating period. After the droplet moves away from the heated surface, both temperatures decrease over time. The left edge cools immediately upon removal of the heat source. The heat conduction rate then decreases across the droplet, thereby allowing the right end of the droplet to cool. The maximum droplet acceleration occurs early in the cycle, when the net force on the droplet reaches a peak value.

Theoretical simulations were performed with time steps of both 5×10^{-9} s and 5×10^{-8} s. Fig. 6 indicates that the results are nearly independent of the time step size. Larger time steps yielded excessive velocities and numerical instability. It can be observed that the peak temperature is higher in the case involving a smaller microchannel (1-μm channel). A specified heat input produces a larger temperature change when the total mass of the micro-droplet is reduced. It appears that the geometrical configuration of the microchannel can be manipulated, in order to produce a desired temperature difference and droplet motion, when a specified heat input is applied to the microchannel.

Fig. 7a shows that the thermocapillary force is nearly identical for each channel during early times. However, the previous results in Fig. 5 suggested that the droplet velocity increases in larger microchannels. In that case, the droplet moves sooner past the stationary heat source, and the earlier cooling causes the edge temperature and thermocapillary force to fall earlier for the largest microchannel (2 μm). Furthermore, the peak temperature at the receding edge of the micro-droplet is reduced when the heating period is shortened.

Microchannels with heights between 0.5 and 2 μm in this section were selected to be smaller than typical microchannels between 10 and 50 μm. Several reasons explain why the microchannels were chosen to be very small. Firstly, generating pressure gradients within the microchannel is a key goal of the micro-system. A given droplet displacement will generate a larger external (air) pressure gradient,

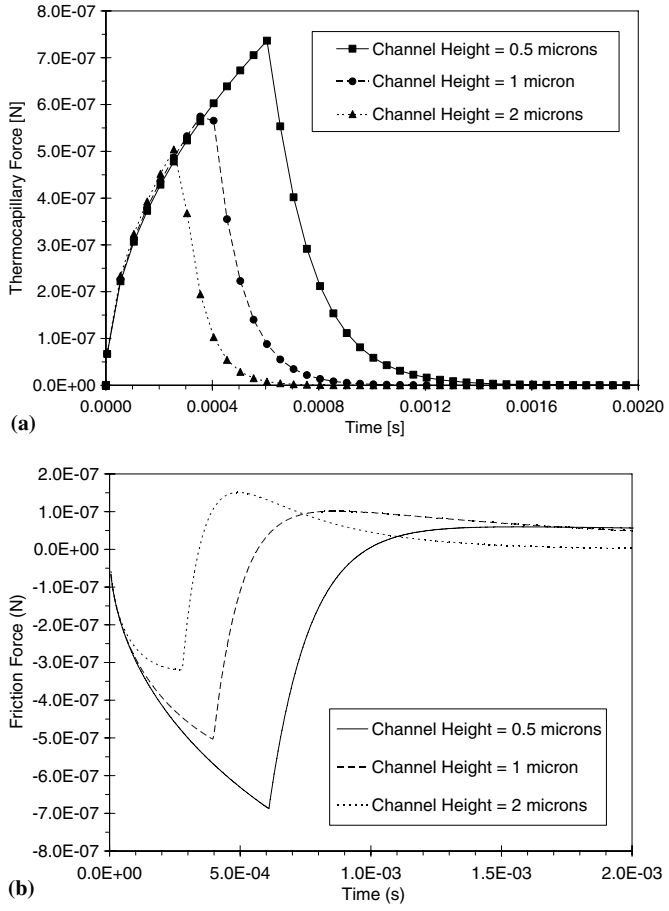

Fig. 7. Comparisons of theoretical predictions of the (a) thermocapillary force and (b) friction force variations over time for varying channel heights.

when a smaller volume of air is compressed. Secondly, the thermocapillary force and resulting thermocapillary pressure of Eq. (18) are inversely proportional to the channel height. Thus, choosing a smaller channel height increases the thermocapillary force for a given temperature difference across the droplet. The larger thermocapillary force, as well as a smaller mass of droplet, increase the droplet acceleration and yield shorter cycle times. Furthermore, the temperature of the heated end of a droplet increases more substantially for smaller droplets when a specified heat flux is applied. Also, the end of the droplet cools faster (due to its reduced mass), thereby allowing it to return faster. These characteristics could have importance in applications requiring high acceleration and frequency of droplet motion.

In Fig. 7b, the frictional drag force is smaller for droplets in larger channels. This is consistent with equations developed in Section 4, which show that the frictional force is inversely proportional to the channel height. Also, the external air force is proportional to the channel height. Although equal droplet displacements yield equal external pressures, the force is directly proportional to the droplet height. When thermocapillary, friction and opposing pressure forces were combined, the resulting net force on the droplet in the largest channel (2 μm) becomes more than four times larger than the force in the smallest channel (0.5 μm). Thus, the droplet in the largest channel will reach a specified position earlier. Also, the acceleration is inversely proportional to the mass of the droplet. Thus, doubling the channel height would require doubling of the net force on the droplet to produce an equivalent droplet displacement.

In Fig. 8, the predicted thermocapillary, friction and external air forces are illustrated during a heating/cooling cycle for the 1-μm channel. The thermocapillary force depicts a similar trend to the previous temperature results. A rising droplet temperature produces a higher thermocapillary force, while an opposite trend occurs with a decreasing temperature during the cooling period. A higher thermocapillary force gnerates a larger pressure gradient and fluid friction within the droplet. As a result, friction forces exhibit a similar trend as thermocapillary forces (see Fig. 8), except that the direction is opposite to the droplet motion. Different trends are observed with the force exerted by the compressed air on the moving droplet. Its magnitude increases during both the heating and early cooling periods, as the gas volume decreases until the droplet velocity becomes zero. At that point, the direction of droplet movement reverses, so the air volume begins expanding and the magnitude of the external air force diminishes. During these periods, the gas force is directed leftwards on the moving droplet, so its magnitude remains negative. However, the magnitude of the friction force changes signs, when the direction of droplet motion reverses.

Additional simulations were performed for comparisons between numerical (FVM; Finite Volume Method) and theoretical formulations (SA Model). In these comparisons, the thermal bridge was excluded from the numerical model and the heat source was a vertically oriented resistance heater aligned with the left edge of the droplet. Fig. 9a shows close agreement between numerical and theoretical results of droplet displacement, except near

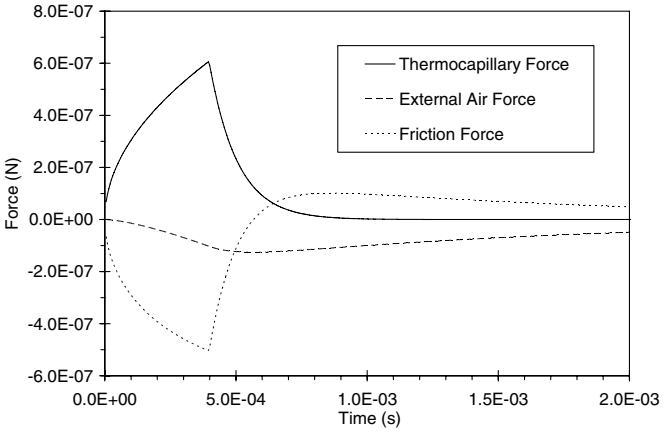

Fig. 8. Comparison of theoretical predictions of forces on accelerating droplet in a closed-ended microchannel for three channel heights.

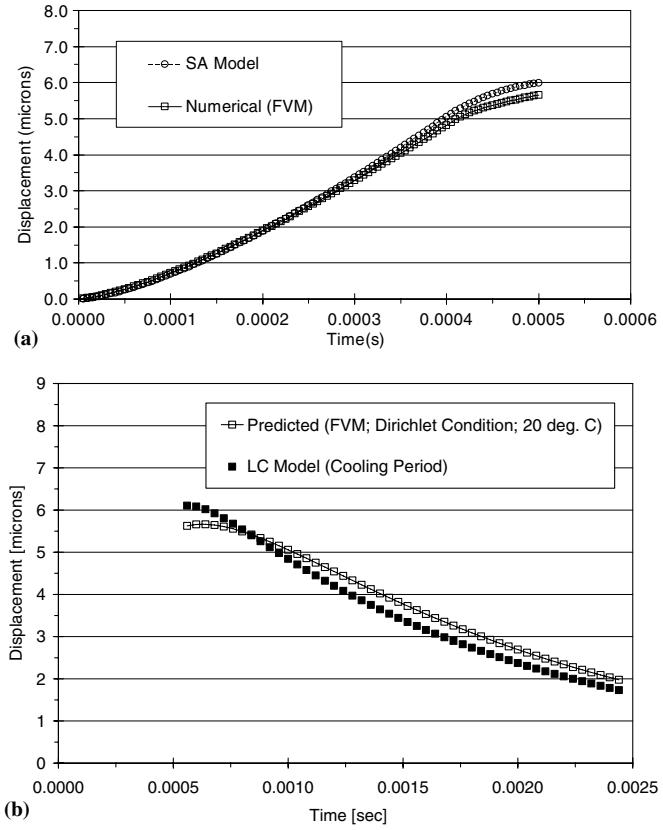

Fig. 9. Comparison of theoretical and numerical predictions of droplet displacement in a closed-ended microchannel during the (a) heating period and (b) cooling period.

the end of the heating period. At that point, the droplet has moved past the heat source and the compressed air exerts an increasing resistance to droplet motion. The one-dimensional theoretical model neglects heat transfer from the substrate to the surroundings, thereby over-predicting the receding edge temperature and thermocapillary force on the droplet. It additionally neglects changes in the air temperature. This leads to small discrepancies between numerical and theoretical results near a time of 0.5 ms in Fig. 9a.

This discrepancy during the heating period affects the initial point of droplet reversal during the cooling period (see Fig. 9b). Nevertheless, reasonable agreement between the SA Model and FVM simulations is achieved in Fig. 9b. During the cooling period, the right gas expands when the droplet moves leftwards. The heat source is turned off during this period. Otherwise, the gas pressure would be insufficient to overcome thermocapillary forces in a heated region near the thermal bridge.

7. Conclusions

In this article, heat transfer and microfluidic forces on a moving droplet within a closed-ended microchannel have been investigated. An external heat source generates thermocapillary forces and pressure differences within the microdroplet, thereby inducing fluid motion against a compressed air region in the microchannel. A theoretical model was developed to predict droplet motion without numerically solving the momentum or energy equations. Temperatures are determined based on an SA Model during heating and a lumped capacitance analysis during the cooling period. Droplet motion is approximated using Newton's Second Law. The thermocapillary force reaches a peak value of about 0.00074 mN during the heating period for a 0.5 μm channel. A lower peak force is predicted at an earlier time when the channel height increases. Furthermore, the magnitude of the friction force reaches about 0.0007 mN, but it decreases when the channel height is enlarged. For all channels, the friction force increases to a local maximum, decreases to a local minimum and approaches zero thereafter, as the droplet returns to its equilibrium position. These trends are considered to have practical utility for effective flow control with thermocapillary pumping in microchannels. Various practical applications may require a periodic cycling of droplet motion within a micro-device, rather than a uniform cycle. In that case, the periods of heating/cooling can be manipulated to establish precise control of droplet displacement. Some examples include matching a resonance frequency or pressure requirement for a thermal switch, optical switch or micro-valve. For such innovative applications and others, this article has provided useful insight regarding thermocapillary forces and droplet transport in a closed-ended microchannel.

Acknowledgements

Support of this research from the Natural Sciences and Engineering Research Council of Canada, as well as a University of Manitoba Graduate Fellowship (P.S. Glockner), is gratefully acknowledged.

References

[1] M. Gad-el-Hak, The fluid mechanics of microdevices – the Freeman Scholar Lecture, ASME J. Fluids Eng. 121 (1999) 5–33.
[2] S. Wu, J. Mai, Y.C. Tai, C.M. Ho, Micro heat exchanger using MEMS impinging jets, in: Proceedings of the 12th Annual International Workshop on Micro Electro Mechanical Systems, Orlando, FL, January 17–21, 1999, pp. 171–176.
[3] K. Vafai, L. Zhu, Analysis of a two-layered channel heat sink concept in electronic cooling, Int. J. Heat Mass Transfer 42 (12) (1999) 2287–2297.
[4] G.F. Naterer, Adaptive surface micro-profiling for microfluidic energy conversion, AIAA J. Thermophys. Heat Transfer 18 (4) (2004) 494–501.
[5] M.J. Martin, I.D. Boyd, Blasius boundary layer solution with slip flow conditions, Paper RGD-11006, in: 22nd Rarefied Gas Dynamics Symposium, Sydney, Australia, 2000.
[6] W. Qu, M. Mala, D. Li, Pressure-driven water flows in trapezoidal silicon microchannels, Int. J. Heat Mass Transfer 42 (2000) 353–364.
[7] M. Mala, D. Li, Flow characteristics of water through microtubes, Int. J. Heat Fluid Flow 20 (1999) 142–148.
[8] C.J. Kim, Micromachines driven by surface tension, AIAA Paper 99-3800, in: AIAA 30th Fluid Dynamics Conference, Norfolk, VA, June 1999, pp. 1–6.
[9] T.S. Sammarco, M.A. Burns, Heat transfer analysis of microfabricated thermocapillary pumping and reaction devices, J. Micromech. Microeng. 10 (2000) 42–55.

[10] J. Lee, C.J. Kim, Theory and modeling of continuous electrowetting microactuation, in: ASME International Mechanical Engineering Congress and Exposition, Proceedings of the MEMS, vol. 1, Nashville, TN, November 1999, pp. 397–403.
[11] T.S. Sammarco, M.A. Burns, Thermocapillary pumping of discrete droplet in microfabricated analysis devices, AIChe J. 45 (2) (2004) 350–366.
[12] O.B. Adeyinka, G.F. Naterer, Modeling of entropy production in turbulent flows, ASME J. Fluids Eng. 126 (6) (2004) 893–899.
[13] A.J. Tudos, G.A.J. Besselink, R.B.M. Schasfoort, Trends in miniaturized total analysis systems for point-of-care testing in clinical chemistry, Lab on a Chip 1 (2001) 83–95.
[14] C.W. Hirt, Thermocapillary sample problems, Technical Report FSI-98-00-TN47, Flow Science Inc., Santa Fe, NM, March 1998.
[15] A.K. Sen, S.H. Davis, Steady thermocapillary flows in two-dimensional slots, J. Fluid Mech. 121 (1982) 163.
[16] G.P. Sasmal, J.I. Hochstein, Marangoni convection with a curved and deforming free surface in a cavity, ASME J. Fluids Eng. 116 (1994) 577.
[17] G.F. Naterer, W. Hendradjit, K.J. Ahn, J.E.S. Venart, Near-wall microlayer evaporation analysis and experimental study of nucleate pool boiling on inclined surfaces, ASME J. Heat Transfer 120 (3) (1998) 641–653.
[18] G.F. Naterer, Heat Transfer in Single and Multiphase Systems, CRC Press, Boca Raton, FL, 2002.
[19] S.V. Patankar, Numerical Heat Transfer and Fluid Flow, Hemisphere Publishing Corporation, 1980.